Magnetic circular dichroism in Fe 2*p* resonant photoemission of magnetite

J. Chen
Department of Physics, National Chung Cheng University, Chia-Yi 621, Taiwan
and National Synchrotron Radiation Research Center, Hsinchu 30077, Taiwan

D. J. Huang
National Synchrotron Radiation Research Center, Hsinchu 30077, Taiwan
and Department of Electrophysics, National Chiao-Tung University, Hsinchu 300, Taiwan

A. Tanaka
Department of Quantum Matters, ADSM, Hiroshima University, Higashi-Hiroshima 739-8526, Japan

C. F. Chang and S. C. Chung
National Synchrotron Radiation Research Center, Hsinchu 30077, Taiwan

W. B. Wu
Department of Electrophysics, National Chiao-Tung University, Hsinchu 300, Taiwan

C. T. Chen
National Synchrotron Radiation Research Center, Hsinchu 30077, Taiwan
and Department of Physics, National Chung Cheng University, Chia-Yi 621, Taiwan

(Received 5 December 2002; revised manuscript received 31 March 2003; published 24 February 2004)

Measurements of magnetic circular dichroism in Fe 2*p* resonant photoemission and calculations based on a full-multiplet cluster model reveal the parameters of the electronic structure of Fe_3O_4. We obtained on-site Coulomb energy U_{dd} of 3*d* electrons, charge-transfer energy Δ which is defined as the energy required to transfer an electron from O 2*p* to Fe 3*d*, and the hybridization strength between Fe 3*d* and O 2*p* at different Fe ion sites of Fe_3O_4 by analyzing the data of magnetic circular dichroism. The charge-transfer energy of Fe^{3+} ions was found to be significantly smaller than that of Fe^{2+} ions. We determined the energy positions of the low-lying multiplets of each Fe ion site. These energy positions for Fe^{3+} ion sites are 1.5–2.5 eV higher than those obtained from band-structure calculations. Our calculations also show that the photoemission spectral weight in binding energy bigger than 10 eV is substantial, in contrast to the results of band-structure calculations. Our findings conclude that Fe_3O_4 is a system with strong electron-electron interactions.

DOI: 10.1103/PhysRevB.69.085107 PACS number(s): 71.28.+d, 75.50.Ss, 75.25.+z, 78.70.Dm

I. INTRODUCTION

Magnetite (Fe_3O_4), a prototype of 3*d* transition-metal compounds with mixed valence, has attracted much attention for the interesting fundamental issues on its physical properties and for its potential applications in future spintronics.[1,2] Fe_3O_4 crystallizes in a cubic inverse spinel structure, in which one-third of the Fe ions are tetrahedrally coordinated with four oxygen ions and the remaining two-thirds of the Fe ions are octahedrally coordinated with six oxygen ions. The tetrahedral and octahedral sites are usually called *A* and *B* sites, respectively. Below 860 K, the magnetic moments of the *A*-site and *B*-site Fe ions are in an antiparallel alignment, forming a ferrimagnet. Fe_3O_4 undergoes a first-order transition at $T_V \sim 120$ K, called the Verwey transition.[3,4] At the temperature below T_V, the crystal symmetry is lowered to monoclinic[5,6] and the conductivity decreases by two orders of magnitude at T_V upon cooling through the transition. Verwey and co-workers interpreted the transition as the ordering of the Fe^{3+} and Fe^{2+} ions at *B* sites driven by electrostatic repulsions. Although intensive studies for more than 60 years, the origin of the transition is still controversial;[7–10] the existence of charge ordering in Fe_3O_4 is being hotly debated.[11–15] The detailed electronic structure of Fe_3O_4 is not well understood yet, although a lot of works have been devoted to this issue.[16–20] First-principles band-structure calculations based on the local density approximation (LDA) predict that Fe_3O_4 is a half-metallic magnet,[21] in which minority-spin electrons are responsible for the conduction, whereas majority-spin electrons are insulating. Some recent experimental results conclude that Fe_3O_4 should be considered as an itinerant magnet and not a fluctuating mixed-valence material.[13–15,22] It is thus an important issue whether the one-particle picture is an appropriate description for the electronic structure of Fe_3O_4.

High-energy spectroscopies such as soft x-ray absorption[23] (XAS) and resonant photoemission[24,25] (RPES) spectroscopies are powerful methods for unraveling the electronic structure of transition-metal oxides because of their symmetry and site selectivity. In particular, magnetic circular dichroism (MCD) provides valuable information on the electronic structure of magnetic materials, as well as the specific alignment of spin sates.[26,27] With the help of multiplet calculations, MCD measurements on Fe_3O_4 can lead us to obtain

detailed information of the $3d$ electronic state on each of the three Fe ion sites separately and the parameters such as on-site Coulomb energy U_{dd} of $3d$ electrons, charge-transfer energy Δ defined as the energy required to transfer an electron from the ligand $2p$ to Fe $3d$, and the hybridization strength between Fe $3d$ and O $2p$.

In this paper, we present measurements of MCD in Fe $2p$ resonant photoemission and in Fe L-edge absorption of high-quality Fe_3O_4 thin films epitaxially grown on MgO(001). Our measurements provide an effective means to extract the parameters of the electronic structure of Fe_3O_4. To analyze the MCD measurements, we performed calculations based on a full-multiplet cluster model. The analysis demonstrates that one can use MCD in resonant core-level spectroscopy to unravel the electronic structure of magnetic materials which contain different spin and oxidation states.

The rest of this paper is organized as follows. In the next section, we briefly describe the experimental details including soft x-ray absorption, resonant photoemission, and epitaxial growth of Fe_3O_4 thin films. The method of multiplet calculations is given in Sec. III. The results and analysis of MCD measurements are presented and discussed in detail in Sec. IV, followed by the conclusions.

II. EXPERIMENTAL DETAILS

We carried out measurements of L-edge XAS and $2p$ resonant photoemission of Fe with the elliptically polarized undulator (EPU) beamline at National Synchrotron Radiation Research Center in Taiwan.[28,29] The EPU can generate circularly polarized light or linearly polarized light with polarization in the horizontal or vertical direction with respect to the storage ring. We measured photoemission spectra with a total energy resolution of 0.4 eV (including photon and electron resolutions) by using a 150-mm-mean-radius hemispherical electron energy analyzer. Photoemission and XAS measurements were carried out with an incident angle 60° and the sample was kept at 300 K in a ultrahigh-vacuum chamber with a pressure in the low-10^{-10}-mbar range. Spectra of Fe L-edge absorption were recorded by detecting the sample drain current with a photon energy resolution of 0.2 eV. Thin films of Fe_3O_4 were grown on MgO(001) single crystals which provide an ideal template for epitaxial growth. The lattice constant of Fe_3O_4, 8.396 Å, is close to twice the MgO lattice constant, 4.211 Å, resulting in an epitaxial growth with a small lattice mismatch. Both the rocksalt structure of MgO and the inverse spinel structure of Fe_3O_4 are based on a fcc oxygen anion lattice, allowing a continuation of the oxygen sublattice over the MgO/Fe_3O_4 interface. We achieved growing epitaxial Fe_3O_4 thin films with evaporating Fe from an effusion cell at the presence of oxygen. Before film growth, the MgO(100) substrate was cleaved *ex-situ* and annealed at a temperature around 650 °C with an oxygen pressure of 5×10^{-8} torr for 1–2 h to remove contamination such as hydrocarbons. The cleanliness and structure of the MgO(100) surface were characterized by photoemission and reflection high-energy electron diffraction (RHEED), respectively. The growth rate of Fe_3O_4 thin films was ~0.5 ML (monolayer) per minute. The structure of the thin films was real-time monitored by RHEED and its thickness was calibrated with the intensity oscillation of the RHEED specular beam. Figures 1(a) and 1(b) show the RHEED images of the MgO substrate and 50-ML Fe_3O_4 thin films grown on MgO(001), respectively. Figure 1(c) depicts the oscillations of the RHEED intensity as a function of growth time. These results reveal that the growth of Fe_3O_4 thin films on MgO(001) is in an epitaxial layer-by-layer mode. The film and its epitaxy were fully characterized by x-ray diffraction. The composition of the film was examined by core-level photoemission and L-edge x-ray absorption of Fe; the results are identical to those obtained from Fe_3O_4 single crystals.

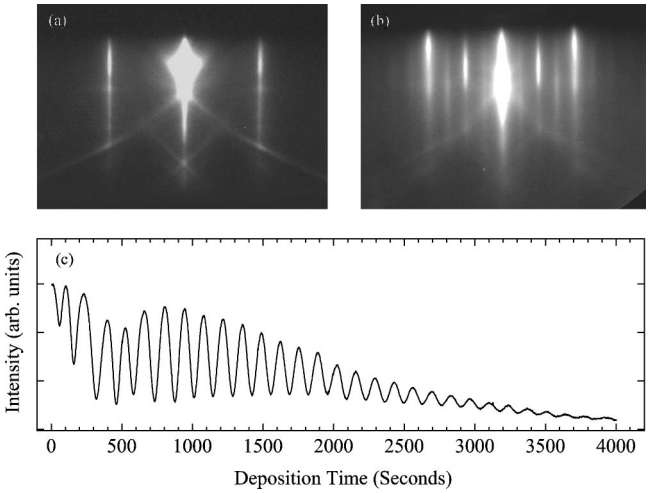

FIG. 1. (a) and (b) RHEED images of a MgO substrate and a 50-ML thin film of Fe_3O_4 grown on MgO(001), respectively. (c) The intensity oscillations of a RHEED specular beam as a function of time during the growth of Fe_3O_4 thin film. The beam energy and incident angle of RHEED were 17 keV and ~0.5°, respectively.

III. METHOD OF CALCULATIONS

With hybridization and charge transfer between Fe $3d$ and O $2p$ taken into consideration, we used a cluster model based on a configuration interaction (CI) approach to calculate the XAS and resonant photoemission spectra of Fe_3O_4.[25,26] We calculated the spectra for each site by exactly diagonalizing the single-ion Hamiltonian under a crystal field where multipole interactions between the $3d$-$3d$ and $3d$-$2p$ cores are described by Slater integrals and a crystal field, and spin-orbit interaction is included. The "nonmultiplet" Hamiltonian describing valence and core states and the effective interaction between electrons are parametrized by the $3d$-$3d$ and $3d$-$2p$ Coulomb interactions (U_{dd} and U_{dc}, respectively) and the hybridization strength between Fe $3d$ and O $2p$. In addition, the charge fluctuation between the ligand $2p$ and cation $3d$ is also taken into account with charge-transfer energy Δ defined as $[E(3d^{n+1}\underline{L})-E(3d^n)]$, where $E(3d^{n+1}\underline{L})$ and $E(3d^n)$ are the average energies of $3d^{n+1}\underline{L}$ and $3d^n$ configurations, respectively.

In the calculation, tetrahedral FeO_4^{5-}, and octahedral FeO_6^{9-} and FeO_6^{10-} clusters corresponding to A-site trivalent Fe ions and B-site trivalent and divalent Fe ions, respec-

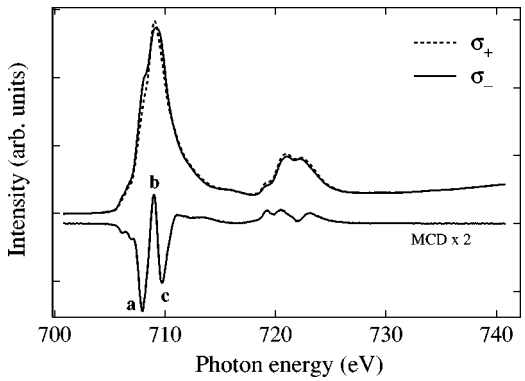

FIG. 2. Fe L-edge XAS and MCD of epitaxial Fe_3O_4/MgO. Upper panel: XAS spectra with spin of photons parallel (denoted as σ_+) and antiparallel (denoted as σ_-) to that of Fe $3d$ majority electrons, respectively. Upper panel: the MCD and MCD integration of the Fe L-edge absorption.

tively, were used. Because of strong Fe $3d$-O $2p$ hybridization, the electronic state of the trivalent Fe ions is described as a linear combination of the $3d^5$, $3d^6\underline{L}$, $3d^7\underline{L}^2$, and $3d^8\underline{L}^3$, where $\underline{L}$ denotes a hole on the oxygen $2p$ orbital and similarly, for the "divalent" Fe ion, $3d^6$, $3d^7\underline{L}$, and $3d^8\underline{L}^2$. The spectra were obtained by making a superposition of those calculated from the above three clusters.

The Hatree-Fock values were adopted for the coupling constants of the $2p$-core and $3d$ spin-orbit interactions and 80% of the values were used for the Slater integrals, which describe the $3d$-$3d$ and $3d$-$2p$ multiplet interactions in the Hamltonian.[30,31] The values of charge-transfer energy Δ, on-site Coulomb energies U_{dd} and U_{dc}, and hopping integrals $[V(t_{2g})$ and $V(e_g)]$ between $3d$ and oxygen $2p$ molecular orbitals were included to reproduce the experimental spectra. In addition, we also used the octahedral crystal field parameter $10Dq=\varepsilon_d(e_g)-\varepsilon_d(t_{2g})$ and hybridization strength between the O $2p$ orbitals $2T_{pp}=\varepsilon_L(e_g)-\varepsilon_L(t_{2g})$ as the calculation parameters. To reduce the number of the free parameters, the empirical relation between Slater-Koster hopping integrals $pd\sigma \approx -4/\sqrt{3}pd\pi$ was assumed. With this assumption, $V(e_g)=-2V(t_{2g})$ for the B site and $V(t_{2g})=\sqrt{3}V(e_g)$ for A site hold. In addition, the Fe-O bond length R dependence of the hopping integral $pd\sigma \propto 1/R^{3.5}$ was further adopted.[32] To emulate the ferrimagnetic order, a small molecular field $H_{\mathrm{mol}}=0.01$ eV was applied to the $3d$ electron spin for each Fe site, which is parallel and antiparallel to the magnetization direction for the B site and A site, respectively.

IV. RESULTS AND DISCUSSIONS

A. XAS of Fe L-edge absorption

We first measured XAS and MCD of Fe L-edge absorption to investigate the electronic structure of magnetite. Figure 2 displays our XAS results of Fe_3O_4 thin films epitaxially grown on MgO(001). XAS spectra with spin of photons parallel (denoted as σ_+) and antiparallel (denoted as σ_-) to that of Fe $3d$ majority electrons were recorded with Fe_3O_4 thin films magnetized remanently along the high-symmetry direction [100]. The incomplete polarization and the incident angle of soft x-ray were corrected with multiplying $(\sigma_+ - \sigma_-)$ by $1/[\cos 60° \times 0.6]$ for MCD spectra. We found that the MCD exhibits a peak at the leading edge of Fe L_3 absorption, denoted as **a**, with a sign opposite to that of the main L_3 absorption peak, denoted as **b**, as shown in Fig. 2. Our results imply that the MCD peak **a** and another MCD peak at higher photon energy, denoted as **c**, originate mainly from the B-site Fe ions and the MCD peak **b** from the A-site Fe^{3+} ions. The absorption peak of the Fe^{2+} ions occurs at a photon energy smaller than that of the Fe^{3+} ions by an energy $\sim(U_{dd}-U_{dc})$—i.e., 1–2 eV toward the low-energy side. We therefore suggest that the leading edge of the L_3 absorption with a negative MCD peak results mainly from the $2p \rightarrow 3d$ transition in the B-site Fe^{2+} ions. In addition, the MCD peak **c** at higher photon energy is derived predominately from the B-site Fe^{3+} ions, consistent with the fact that the magnetic moments of the A-site and B-site Fe atoms are in antiparallel alignment. To obtain the parameters of the electronic structure of Fe_3O_4, we resort to measurements and calculations of Fe $2p$ resonant photoemission.

B. MCD in Fe $2p$ resonant photoemission

Resonant photoemission excited by photons with energy near the absorption threshold of a core level such as $2p$ is a useful technique for the investigation of valence-band features in solids. In particular, one can use MCD in resonant photoemission to determine the parameters of the detailed electronic structure of compounds such as Fe_3O_4 containing compositions of different spin directions. Figure 3 shows resonant-photoemission spectra of Fe_3O_4 excited by photons which give rise to three distinct peaks (denoted as **a**, **b**, and **c**) in the spectra of MCD in absorption. With the photon energy corresponding to the peak **a** of MCD in absorption, the resonance process enhances the intensities of photoelectrons corresponding to the final-state configurations of $3d^5$, $3d^6\underline{L}$, and $3d^7\underline{L}^2$ of B-site Fe ions. If the photons are tuned at energies corresponding to the peaks **b** and **c** of MCD in absorption, the intensities of photoelectrons arising from the final-state configurations of $3d^4$, $3d^5\underline{L}$, and $3d^6\underline{L}^2$ of A-site and B-site Fe ions are enhanced, respectively. The resonant photoemission spectra were taken with photon spin parallel and antiparallel to that of Fe $3d$ majority electrons; the difference spectra—i.e., MCD in resonant photoemission—provide us with great opportunities to unravel the electronic structure of Fe ions with well-defined spin. Figure 3 shows also MCD in Fe $2p$ resonant photoemission excited by photons of different energies. With photons tuned at the peak **b** of MCD in absorption, the sign of MCD in resonant photoemission from the valence band is opposite to those with photons at peaks **a** and **c**, consistent with the measurements of MCD in Fe L-edge absorption, showing that Fe_3O_4 is a ferrimagnet.

To unravel the parameters of Fe_3O_4, we calculated resonant photoemission spectra, as shown in Fig. 4, based on a CI approach. The upper panels of Fig. 4(a), Fig. 4(b), and Fig. 4(c) show the calculated resonant photoemission spectra

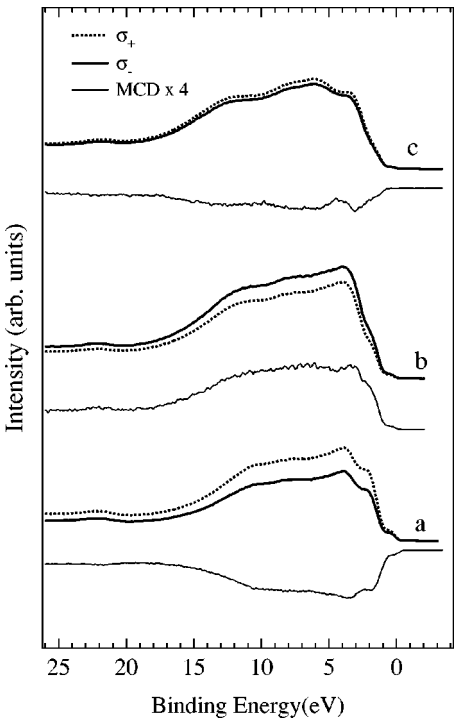

FIG. 3. Resonant photoemission spectra of Fe_3O_4 excited by circularly polarized photons with energies corresponding to the peaks **a**, **b**, and **c** of the MCD in Fe *L*-edge absorption as described in the text. The background of RPES spectra has been removed by using a Shirely background function. The MCD in resonant photoemission are shown as thin solid lines. The spectra are with different vertical offsets for clarity.

with photon energies corresponding to the MCD peaks **a**, **b**, and **c**, respectively. The spectra were broadened by a Gaussian full width at half maximum (FWHM) of 0.4 eV for instrumental broadening and by a Lorentian FWHM of 0.2 eV for lifetime broadening. Table I shows the parameters used in the calculations. To reduce the number of parameters, we adopted the same parameter of hybridization strength for the *B*-site Fe^{2+} and Fe^{3+} because they coexist in the same octahedral surrounding of ligands.

TABLE I. Parameters in units of eV for the electronic structure of Fe_3O_4 used in the cluster-model calculations. The charge-transfer energy Δ, the on-site $3d$-$3d$ Coulomb energy U_{dd}, and the $3d$-$2p$ Coulomb energy U_{dc} on Fe ions, the hybridization strength between Fe $3d$ and O $2p$ $V(e_g)$, the O_h crystal field $10Dq$, and the hybridization strength between O $2p$ orbitals T_{pp}.

	Δ	U_{dd}	U_{dc}	$V(e_g)$	$10Dq$	T_{pp}
B-site Fe^{2+}	7.0	6.0	7.5	2.1	0.5	0.7
B-site Fe^{3+}	1.0	6.0	7.5	2.1	0.7	0.7
A-site Fe^{3+}	3.5	6.0	7.5	1.34	−0.7	0

Now we discuss the detailed structure of the spectra. For *B*-site Fe^{3+} [see Fig. 4(c)], the average energy of the $3d^4$ final state is 5 eV (i.e., $U_{dd}-\Delta$) higher than that of the $3d^5\underline{L}$ state, if there were no hybridization. Because of strong Fe $3d$-O $2p$ hybridization, some of the $3d^5\underline{L}$ states are coupled with the $3d^4$ states and are pushed out to the low-binding-energy side. As a result, the spectra of *B*-site Fe^{3+} consist of three structures: the nonbonding $3d^5\underline{L}$ peak placed about 7.5 eV, the structure at the low binding energy <6.5 eV arising from the bonding state of $3d^4$ and $3d^5\underline{L}$ states, and the broad antibonding satellite centered around 13 eV. The energy level scheme of the low-lying multiplets is the same as that of a pure Fe^{4+} ion placed in the crystal field with O_h symmetry. The low-binding-energy structure found in the *B*-site Fe^{3+} spectra in Fig. 4(c) consist of such multiplets ^5E and $^5T_2$. These multiplets can be reached by removal of the $e_{g\uparrow}$ and $t_{2g\uparrow}$ electrons from the $^6A_1$ ground state mainly consisting of

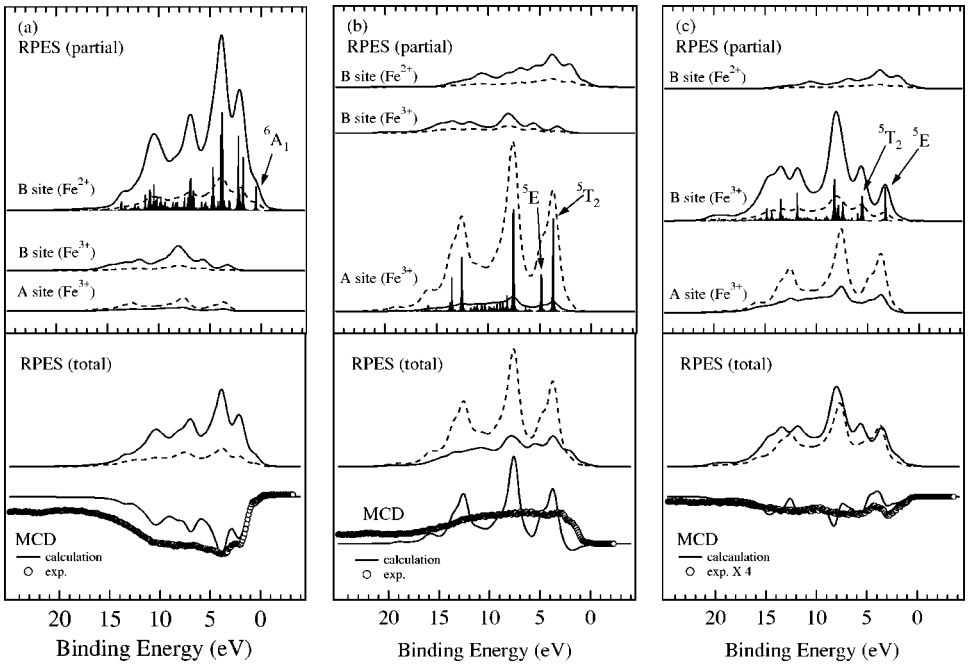

FIG. 4. Calculated resonant photoemission and MCD spectra of Fe_3O_4. Partial resonant photoemission spectra excited with energies corresponding to the peaks **a**, **b**, and **c** of the MCD in Fe *L*-edge absorption are shown in (a), (b), and (c), respectively. The calculated (solid lines) and the measured MCD (open circles) in Fe $2p$ resonant photoemission are shown in the lower panels. The descriptions of the figure correspond to those of Fig. 3. The vertical sticks show the calculated spectra without broadening. All measured MCD are multiplied by $1/[\cos 60° \times 0.6]$ as explained in the text.

a $t_{2g\uparrow}^3 e_{g\uparrow}^2$ configuration and the energy difference of the two corresponds to the effective $10Dq$ value. The spectrum for *A*-site Fe^{3+} is also similar to that for *B*-site; however, since the effective $10Dq$ value is negative for this site, the energy positions of the two multiplets ^5E and $^5T_2$ are reversed. Analogous to the above discussion, for the *B*-site Fe^{2+} ion [see Fig. 4(a)], the nonbonding $3d^6\underline{L}$ peak located around $\sim$7.5 eV and the multiplet structure ($<$5 eV) arising from the bonding state of the $3d^5$ and $3d^6\underline{L}$ and the shoulder structure around $\sim$10 eV corresponding to the antibonding state of the two can be found. The structure in the vicinity of the Fermi level ($\sim$0.5 eV) corresponds to the multiplet $^6A_1$, which can be reached by removal of the $t_{2g\downarrow}$ electron from the $^5T_2$ ground state mainly consisting of the $t_{2g\uparrow}^3 e_{g\uparrow}^2 t_{2g\downarrow}^1$ configuration. Note that since the average energy difference between the $3d^5$ and $3d^6\underline{L}$ configurations is only 1 eV, the $^6A_1$ state at the valence top is a strong mixture of the $3d^5$ and $3d^6\underline{L}$ states.

We plot also the measured and calculated MCD in Fe $2p$ resonant photoemission in the lower panels of Fig. 4. All measured MCD are multiplied by $1/[\cos 60° \times 0.6]$ to account for the incomplete polarization and the incident angle of photons. The calculated spectra resemble most of main peak positions of the measurements with photons tuned at the peaks **a** and **c** of MCD in XAS, but have much narrower widths than those of measurements because band effects are not taken into account in the calculations. Comparison between calculations and measurements shows that MCD obtained with photons tuned at peak **c** is strongly reduced, indicating that the Fe L_3 absorption energies for *A*-site and *B*-site Fe^{3+} ions are close to each other. As a result, the calculations yield comparable partial resonant photoemission spectra of these two sites excited by photons with an energy corresponding to peak **c**, as shown in the lower panel of Fig. 4(c). For resonant photoemission with photon energy corresponding to the peak **b** of MCD in XAS, the calculated MCD peaks are pronounced and their intensities are significantly larger than the measured ones. One must recognize that the measure resonant photoemission spectra were taken with a photon energy resolution of 0.3 eV, whereas the calculations were performed with excitation photons of a well-defined energy. In particular, the measured resonant photoemission spectrum with photons tuned at peak **b** originates from *A*-site Fe^{2+} ions with a strong mixture of *B*-site Fe^{3+} and Fe^{2+} ions, resulting from a finite photon energy width; the measured MCD spectrum is therefore smeared out and its intensity is strongly reduced because of antiparallel alignment of *A*-site and *B*-site magnetic moments. In addition, incoherent Auger electrons contribute to the background of resonant photoemission spectra, especially for those excited by photons with an energy higher than that corresponding to peak **a**; consequently, the intensities of measured MCD spectra are further reduced.

We found that the charge-transfer energy of the *B*-site Fe^{2+} ions is significantly larger than that of the *B*-site Fe^{3+} ions. The charge-transfer energy Δ is related to the on-site $3d$ Coulomb energy and the difference in Madelung potential between the Fe and O sites. The charge-transfer energy, defined with respect to the center of gravity of each multiplet, is given by

$$\Delta = \varepsilon_d^0 - nU_{dd} - \varepsilon_L^0, \tag{1}$$

where $\varepsilon_d^0 = \frac{1}{5}[2\varepsilon_d(e_g) + 3\varepsilon_d(t_{2g})]$ and $\varepsilon_L^0 = \frac{1}{5}[2\varepsilon_L(e_g) + 3\varepsilon_L(t_{2g})]$ are the bare energy of the $3d$ orbital and O $2p$ orbital, respectively, including the Madelung potential.[34] The change in $\varepsilon_d^0 - \varepsilon_L^0$ and that in nU_{dd} lead to a variation of the charge-transfer energy. When going from a divalent to a trivalent Fe ion, Δ decreases by $U_{dd} + \Delta V_M(Fe^{2+}) - \Delta V_M(Fe^{3+})$ where ΔV_M is the Madelung potential difference between the Fe and O sites. From the viewpoint of the point charge model, the Madelung energy of the oxygen site in a FeO_6 octahedron is determined by the valence of Fe and the Fe-O bond length. Although the oxygen sites bonding with *B*-site Fe^{2+} and Fe^{3+} have the same valence, the difference in the Fe-O bond length also contributes to the Madelung energy of the oxygen site. The true Madelung energy in a real solid is hardly estimated quantitatively. In addition, the characters of covalency of Fe_3O_4 above the Verwey transition might lead to a reduction of the Madelung energy difference between Fe and O for *B*-site Fe^{2+} and Fe^{3+}. As a result of covalency effects, this difference in Madelung energy is considerably smaller than the value estimated from the point charge model.[33] Our results indicate that the difference between the charge-transfer energy of Fe^{2+} and that of Fe^{3+} is $\sim U_{dd}$, consistent with the fact that Fe^{2+} and Fe^{3+} coexist in the same octahedral surrounding of ligands.

TABLE II. The weight of the configurations $w(d^n)$, the number of $3d$ electrons n_{3d} in the ground state for three different sites obtained with the cluster model.

	A-site Fe^{3+}	*B*-site Fe^{2+}	*B*-site Fe^{3+}
$w(d^5)$	72.2%	-	58.0%
$w(d^6)$	25.7%	84.8%	37.6%
$w(d^7)$	2.1%	14.7%	4.3%
$w(d^8)$	0.0%	0.5%	0.1%
n_{3d}	5.30	6.15	5.47

To discuss the covalent feature of Fe_3O_4, we show the weight of the configurations and the $3d$ electron number in the ground state for each Fe site in Table II. Because of small charge-transfer energy, the weight of the configuration $3d^6\underline{L}$ for the trivalent Fe ions, especially the *B*-site Fe^{3+}, are large, showing a strong covalent feature. In addition, the difference in the $3d$ electron number between Fe^{2+} and Fe^{3+} ions at the *B* site is only 0.68. The low-energy multiplet level scheme is the same as that for the pure Fe^{3+} ion in a crystal field, although with such a strong Fe $3d$-O $2p$ hybridization.

C. Partial density of states of $3d$ states

We also calculated the partial density of states (DOS) of the $3d$ orbitals with the same parameter set obtained above.

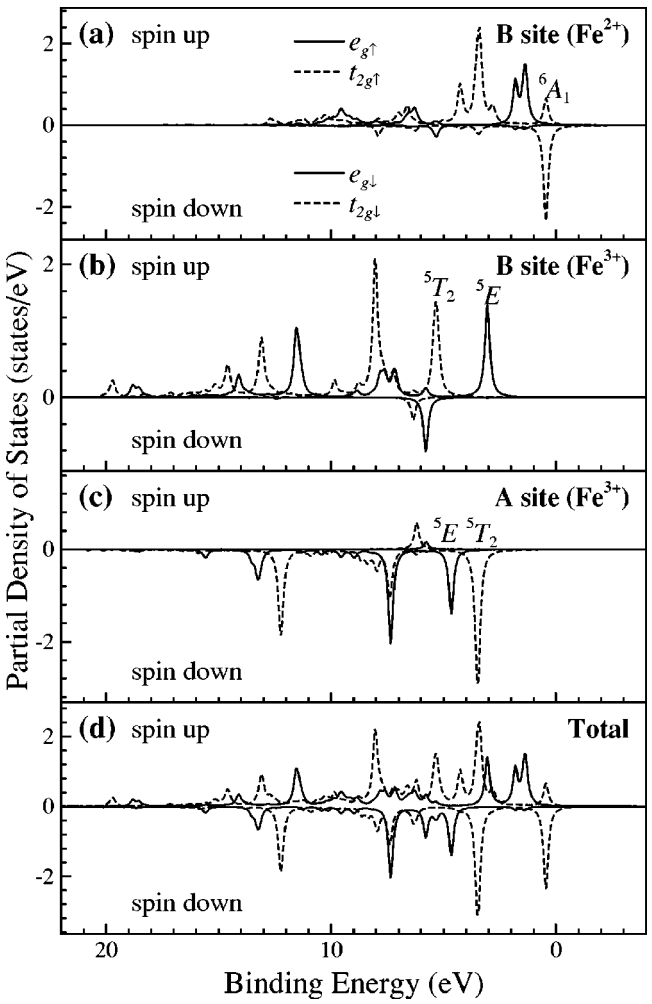

FIG. 5. Partial DOS of *B*-site Fe^{2+} ions (a), *B*-site Fe^{3+} ions (b), and *A*-site Fe^{3+} ions (c) and the total over the three sites (d) are shown obtained with the cluster model using the parameter set in Table I. In each panel, the partial DOS of the e_g (solid line) and t_{2g} (dashed line) symmetry orbitals with up spin and down spin are depicted.

The partial DOS of the $3d$ orbitals $\rho_{\Gamma,\sigma}(E_B)$ with $\Gamma=e_g$ or $\Gamma=t_{2g}$ symmetries for a spin σ at binding energy E_B is defined by

$$\rho_{\Gamma,\sigma}(E_B)=\sum_{f,\gamma\in\Gamma}|\langle f|d_{\gamma,\sigma}|g\rangle|^2\delta(E_f-E_B)$$
$$=\sum_{\gamma\in\Gamma}\frac{1}{\pi}\mathrm{Im}\left\langle g\left|d^{\dagger}_{\gamma,\sigma}\frac{1}{H_f-E_B-i\delta}d_{\gamma,\sigma}\right|g\right\rangle, \quad (2)$$

where E_f and H_f are the eigenenergy and Hamiltonian of the final state of photoemission (one-electron removal state), respectively; γ runs over the t_{2g} orbitals for $\Gamma=t_{2g}$ and the e_g orbitals for $\Gamma=e_g$. Note that the sum $\rho_{e_g\uparrow}+\rho_{e_g\downarrow}+\rho_{t_{2g}\uparrow}+\rho_{t_{2g}\downarrow}$ corresponds to the $3d$ cross section of nonresonant photoemission.

Figure 5 shows the partial DOS of the $3d$ orbitals with the e_g (solid line) and t_{2g} (dashed line) symmetries for up spin and down spin. The upper three panels show the partial DOS for each Fe ion site separately, and in the bottom, the sum over the three sites is depicted. The partial DOS are broadened with a lifetime width $\delta=0.1$ eV and a Guassian width 0.2 eV. In band-structure calculations of Fe_3O_4, the $t_{2g\downarrow}$ band in the *B* site is positioned at the Fermi level,[9,21] in accordance with our calculation, where the $t_{2g\downarrow}$ peak originating from the $^6A_1$ multiplet is situated in the vicinity of the Fermi level [see Fig. 5(a)]. The structures around $\sim$1.5 eV in $\rho_{e_g\uparrow}$ and $\sim$3.5 eV in $\rho_{t_{2g}\uparrow}$ for *B*-site Fe^{2+} ions correspond to the $e_{g\uparrow}$ and $t_{2g\uparrow}$ bands in the band-structure calculations,[21] respectively. In addition, the peaks located at energies of 3 eV and 5.3 eV in Fig. 5(b) arise from the ^5E and $^5T_2$ multiplets in the partial DOS for *B*-site Fe^{3+} ions, respectively, which are also $e_{g\uparrow}$ and $t_{2g\uparrow}$ removal states, respectively [see Fig. 5(b)]. The binding energies of these states are $\sim$1.5 eV higher than those of *B*-site Fe^{2+} ions and are also 1.5–2.5 eV higher, as compared to the $e_{g\uparrow}$ and $t_{2g\uparrow}$ band energies from band-structure calculations.[21] The ^5E and $^5T_2$ multiplet peaks in the partial DOS for *A*-site Fe^{3+} ions correspond to the $e_{g\uparrow}$ and $t_{2g\uparrow}$ states, respectively. The energies of these multiplets are also located at 1.5–2.5 eV higher than corresponding band energies.[21]

The structures around 7.5 eV in the partial DOS of Fe^{3+} ions arise from the nonbonding $3d^5\underline{L}$ states, which are situated in the O $2p$ band. These have a large intensity because of strong final-state multiplet interactions. In a binding energy higher than 10 eV, the antibonding structures, which are totally absent in the band-structure calculations, have substantial intensities in both our calculations and experimental resonant and nonresonant[19] photoemission spectra. Our calculations also provide better energy positions for the low-lying $3d$ states of Fe^{3+} ion sites. We therefore suggest that Fe_3O_4 is a system with strong electron-electron interactions.

D. MCD in Fe *L*-edge absorption

With the parameters shown in Table I, we analyzed the $L_{2,3}$ absorption spectra of Fe_3O_4 measured by using photons with left and right circular polarization to further check the parameters described above. The $2p$ XAS spectrum reflects directly the nature of the $3d$ electronic ground state. The local ground state of Fe ions is a mixture of configurations $3d^n$, $3d^{n+1}\underline{L}$, and $3d^{n+2}\underline{L}^2$ with $n=5$ and $n=6$ for Fe^{3+} and Fe^{2+} ions, respectively. The final state in *L*-edge absorption is predominantly a mixture of configurations $\underline{2p}3d^{n+1}$ and $\underline{2p}3d^{n+2}\underline{L}$. The $\underline{2p}3d^{n+1}$ configuration exhibits multiplet structure as a consequence of the $2p$-$3d$ exchange interaction, whereas a broadband feature exists in the configuration $\underline{2p}3d^{n+2}\underline{L}$ resulting from the bandlike character of the ligand hole.

MCD spectra provide a deeper insight in the excitation process, because MCD spectra contain specific information about the alignment of the spin and orbital moments in the final states. With solid lines for spectra excited by photons with spin parallel to that of Fe $3d$ majority electrons and dashed lines for antiparallel alignment, Fig. 6 shows the XAS and MCD of each Fe site. XAS spectra of *A*-site Fe^{3+},

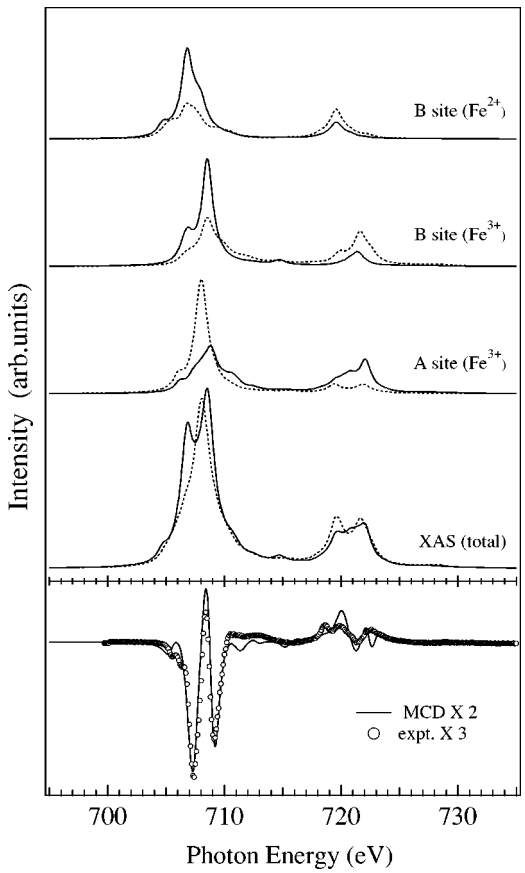

FIG. 6. Upper panel: calculated XAS spectra of *B*-site Fe^{2+}, *B*-site Fe^{3+}, and *A*-site Fe^{3+} ions and the total obtained from the cluster-model. The descriptions of the figure correspond to those of Fig. 2. The parameters used in the calculations are shown in Table I. Lower panel: calculated total MCD spectrum (solid line) and experimental MCD data (circles) are show.

B-site Fe^{3+}, and *B*-site Fe^{2+} ions were separately calculated. The difference in the average energy of the $2p3d^6$ configuration of *B*-site Fe^{3+} ions and the $2p3d^7$ configuration of *B*-site Fe^{2+} ions in the absence of hybridization is $U_{dd}-U_{dc}=1.5$ eV and the average energy of the $2p3d^6$ configuration of *A*-site Fe^{3+} ions is chosen to be 0.5 eV lower than that of *B*-site Fe^{3+} ions so to fit the experimental MCD spectrum in the L_3 region. Similar to the previous multiplet calculations of MCD in Fe *L*-edge absorption of Fe_3O_4,[34,35] we are able to reproduce MCD spectra exhibiting most of the features in the MCD measurements. The measured MCD is smaller than that of calculations by a factor of 1.5, because of band formation and lack of a single magnetic domain. With magnetic hysteresis measurements, we found that the remanent magnetization is 80% of the saturation magnetization. This comparison indicates that we have a reasonable and consistent picture of the parameters for the electronic structure of Fe_3O_4.

V. CONCLUSIONS

We combined measurements of magnetic circular dichroism in core-level spectroscopy and multiplet calculations to unravel the parameters of the electronic structure of Fe_3O_4 such as on-site $3d$ Coulomb energy U_{dd}, charge-transfer energy Δ, and the hybridization strength between Fe $3d$ and O $2p$ of specific spin states in Fe_3O_4. We obtained a large value of $U_{dd}\sim 6$ eV and found that the charge-transfer energy of Fe^{3+} ions is significantly smaller that of Fe^{2+} ions. We also determined the energy positions of the multiplets at the lowest binding energy for each ion site. The energy positions for Fe^{3+} ion sites are found to be 1.5–2.5 eV higher than the results of band-structure calculations. Our calculations also show that the photoemission spectral weight with a binding energy bigger than 10 eV is still substantial, in contrast to the results of band-structure calculations. These results indicate that Fe_3O_4 is a system with strong electron-electron interactions.

ACKNOWLEDGMENTS

We thank L. H. Tjeng for valuable discussions. This work was supported in part by the National Science Council of Taiwan under Contract Nos. NSC91-2112-M-213-018 and NSC91-2112-M-213-009.

[1] M. Imada, A. Fujimori, and Y. Tokura, Rev. Mod. Phys. **70**, 1039 (1998).
[2] N. Tsuda, K. Nasu, A. Fujimori, and K. Shiratori, *Electronic Conduction in Oxides*, 2nd ed. (Springer-Verlag, Berlin, 2000), p. 243.
[3] E.J.W. Verwey, Nature (London) **144**, 327 (1939).
[4] E.J.W. Verwey and P.W. Haayman, Physica (Amsterdam) **8**, 979 (1941).
[5] J. Yoshida and S. Iida, J. Phys. Soc. Jpn. **42**, 230 (1977); S. Iida, Philos. Mag. B **42**, 349 (1980).
[6] M. Iizumi, T.F. Koetzle, G. Shirane, S. Chikazumi, M. Matsui, and S. Todo, Acta Crystallogr., Sect. B: Struct. Crystallogr. Cryst. Chem. **38**, 2121 (1982).
[7] J.R. Cullen and E.R. Callen, Phys. Rev. B **7**, 397 (1973).
[8] D. Ihle and B. Lorentz, J. Phys. C **18**, L645 (1985).
[9] V.I. Anisimov, I.S. Elfimov, N. Hamada, and K. Terakura, Phys. Rev. B **54**, 4387 (1996).
[10] H. Seo, M. Ogata, and H. Fukuyama, Phys. Rev. B **65**, 085107 (2002).
[11] J.P. Wright, J.P. Attfield, and P.G. Radaelli, Phys. Rev. Lett. **87**, 266401 (2001).
[12] M. Mizoguchi, J. Phys. Soc. Jpn. **70**, 2333 (2001).
[13] P. Novak, H. Stepankova, J. Englich, J. Kohout, and V.A.M. Brabers, Phys. Rev. B **61**, 1256 (2000).
[14] J. Garcia, G. Subias, M.G. Proietti, H. Renevier, Y. Joly, J.L. Hodeau, J. Blasco, M.C. Sanchez, and J.F. Berar, Phys. Rev. Lett. **85**, 578 (2000).
[15] J. Garcia, G. Subias, M.G. Proietti, J. Blasco, H. Renevier, J.L. Hodeau, and Y. Joly, Phys. Rev. B **63**, 054110 (2001).
[16] S.F. Alvarado, W. Eib, F. Meier, D.T. Pierce, K. Sattler, H.C.

Siegmann, and J.P. Remeika, Phys. Rev. Lett. **34**, 319 (1975).
[17] A. Chainani, T. Yokoya, T. Morimoto, T. Takahashi, and S. Todo, Phys. Rev. B **51**, 17 976 (1995).
[18] J.-H. Park, L.H. Tjeng, J.W. Allen, P. Metcalf, and C.T. Chen, Phys. Rev. B **55**, 12 813 (1997).
[19] D.J. Huang, C.F. Chang, J. Chen, L.H. Tjeng, A.D. Rata, W.P. Wu, S.C. Chung, H.J. Lin, T. Hibma, and C.T. Chen, J. Magn. Magn. Mater. **239**, 261 (2002).
[20] Y.S. Dedkov, U. Rüdiger, and G. Güntherodt, Phys. Rev. B **65**, 064417 (2002).
[21] H.-T. Jeng and G.Y. Guo, Phys. Rev. B **65**, 094429 (2002), references therein.
[22] K. Siratori, Y. Ishii, Y. Morii, and S. Funahashi, J. Phys. Soc. Jpn. **67**, 2818 (1998).
[23] *Unoccupied Electronic States*, edited by J.C. Fuggle and J.E. Inglesfield (Springer-Verlag, Berlin, 1992).
[24] L.H. Tjeng, C.T. Chen, J. Ghijsen, P. Rudolf, and F. Sette, Phys. Rev. Lett. **67**, 501 (1991).
[25] A. Tanaka and T. Jo, J. Phys. Soc. Jpn. **63**, 2788 (1994).
[26] A. Tanaka and T. Jo, J. Phys. Soc. Jpn. **61**, 2669 (1992).
[27] G. van der Laan, C.M.B. Henderson, R.A.D. Pattrick, S.S. Dhesi, P.F. Schofield, E. Dudzik, and D.J. Vaughan, Phys. Rev. B **59**, 4314 (1999).
[28] C.S. Hwang and S. Yeh, Nucl. Instrum. Methods Phys. Res. A **420**, 29 (1999).
[29] S.-C. Chung, J. Chen, L.-R. Huang, R.T. Wu, C.-C. Chen, N.-F. Cheng, J. M. Chuang, P.-C. Tseng, D.-J. Huang, C. F. Chang, S.-Y. Perng, C.T. Chen, and K.-L. Tsang, Nucl. Instrum. Methods Phys. Res. A **467**, 445 (2001).
[30] F.M.F. de Groot, J.C. Fuggle, B.T. Thole, and G.A. Sawatzky, Phys. Rev. B **42**, 5459 (1990).
[31] T. Uozumi, K. Okada, A. Kotani, R. Zimmermann, P. Steiner, S. Hüfner, Y. Tezuka, and S. Shin, J. Electron Spectrosc. Relat. Phenom. **83**, 9 (1997).
[32] W. A. Harrison, *Electronic Structure and Physical Properties of Solids* (Freeman, San Francisco, 1980).
[33] A. Fujimori, A.E. Bocquet, T. Saitoh, and T. Mizokawa, J. Electron Spectrosc. Relat. Phenom. **62**, 141 (1993).
[34] P. Kuiper, B.G. Searle, L.-C. Duda, R.M. Wolf, and P.J. van der Zaag, J. Electron Spectrosc. Relat. Phenom. **86**, 107 (1997).
[35] A. Mirone and M. Sacchi, Phys. Rev. B **61**, 13 540 (2000).